Quantitative monitoring of laser-treated engineered skin using optical coherence tomography

Yujin Ahn,[1] Chan-Young Lee,[1] Songyee Baek,[1] Taeho Kim,[2] Pilun Kim,[3] Sunghoon Lee,[4] Daejin Min,[4] Haekwang Lee,[4] Jeehyun Kim,[5] and Woonggyu Jung[1,6,*]

[1]*Department of Biomedical Engineering, Ulsan National Institute of Science and Technology (UNIST), Ulsan, 44919, South Korea*

[2]*FuturIST Co., Ltd., Ulsan, 44610, South Korea*
[3]*Oz-Tec Co., Ltd., Daegu, 41566, South Korea*
[4]*Amorepacific R&D center, Yongin, 17074, South Korea*
[5]*School of Electronics Engineering, Kyungpook National University, Daegu, 41566, South Korea*
[6]*Center of Soft and Living Matter, Institute for Basic Science (IBS), Ulsan, 44919, South Korea*
[*]*wgjung@unist.ac.kr*

Abstract: Nowadays, laser therapy is a common method for treating various dermatological troubles such as acne and wrinkles because of its efficient and immediate skin enhancement. Although laser treatment has become a routine procedure in medical and cosmetic fields, the prevention of side-effects, such as hyperpigmentation, redness and burning, still remains a critical issue that needs to be addressed. In order to reduce the side-effects while attaining efficient therapeutic outcomes, it is essential to understand the light-skin interaction through evaluation of physiological changes before and after laser therapy. In this study, we introduce a quantitative tissue monitoring method based on optical coherence tomography (OCT) for the evaluation of tissue regeneration after laser irradiation. To create a skin injury model, we applied a fractional CO_2 laser on a customized engineered skin model, which is analogous to human skin in terms of its basic biological function and morphology. The irradiated region in the skin was then imaged by a high-speed OCT system, and its morphologic changes were analyzed by automatic segmentation software. Volumetric OCT images in the laser treated area clearly visualized the wound healing progress at different time points and provided comprehensive information which cannot be acquired through conventional monitoring methods. The results showed that the laser wound in engineered skins was mostly recovered from within 1~2 days with a fast recovery time in the vertical direction. However, the entire recovery period varied widely depending on laser doses and skin type. Our results also indicated that OCT-guided laser therapy would be a very promising protocol for optimizing laser treatment for skin therapy.

References and links

1. T. Hakozaki, C. L. Swanson, and D. L. Bissett, *Textbook of Aging Skin* (Springer, 2010), Chap. 51.
2. Y. R. Helfrich, D. L. Sachs, and J. J. Voorhees, "Overview of skin aging and photoaging," Dermatol. Nurs. **20**(3), 177–184 (2008).
3. G. Overton, D. A. Belforte, A. Nogee, and C. Holton, "Laser Marketplace 2015: Lasers surround us in the Year of Light," http://www.laserfocusworld.com/articles/print/volume-51/issue-01/features/laser-marketplace-2015-lasers-surround-us-in-the-year-of-light.html.

4. L. J. Bernstein, A. N. Kauvar, M. C. Grossman, and R. G. Geronemus, "The short- and long-term side effects of carbon dioxide laser resurfacing," Dermatol. Surg. **23**(7), 519–525 (1997).
5. E. M. Graber, E. L. Tanzi, and T. S. Alster, "Side effects and complications of fractional laser photothermolysis: experience with 961 treatments," Dermatol. Surg. **34**(3), 301–307 (2008).
6. W. M. Petroll, H. D. Cavanagh, and J. V. Jester, "Dynamic three-dimensional visualization of collagen matrix remodeling and cytoskeletal organization in living corneal fibroblasts," Scanning **26**(1), 1–10 (2004).
7. S. J. Lin, R. Wu, Jr., H. Y. Tan, W. Lo, W. C. Lin, T. H. Young, C. J. Hsu, J. S. Chen, S. H. Jee, and C. Y. Dong, "Evaluating cutaneous photoaging by use of multiphoton fluorescence and second-harmonic generation microscopy," Opt. Lett. **30**(17), 2275–2277 (2005).
8. P. Calzavara-Pinton, C. Longo, M. Venturini, R. Sala, and G. Pellacani, "Reflectance confocal microscopy for *in vivo* skin imaging," Photochem. Photobiol. **84**(6), 1421–1430 (2008).
9. E. Brown, T. McKee, E. diTomaso, A. Pluen, B. Seed, Y. Boucher, and R. K. Jain, "Dynamic imaging of collagen and its modulation in tumors *in vivo* using second-harmonic generation," Nat. Med. **9**(6), 796–801 (2003).
10. D. Huang, E. A. Swanson, C. P. Lin, J. S. Schuman, W. G. Stinson, W. Chang, M. R. Hee, T. Flotte, K. Gregory, C. A. Puliafito, and J. G. Fujimoto, "Optical coherence tomography," Science **254**(5035), 1178–1181 (1991).
11. J. Welzel, E. Lankenau, R. Birngruber, and R. Engelhardt, "Optical coherence tomography of the human skin," J. Am. Acad. Dermatol. **37**(6), 958–963 (1997).
12. W. Wieser, W. Draxinger, T. Klein, S. Karpf, T. Pfeiffer, and R. Huber, "High definition live 3D-OCT *in vivo*: design and evaluation of a 4D OCT engine with 1 GVoxel/s," Biomed. Opt. Express **5**(9), 2963–2977 (2014).
13. D. Xu, Y. Huang, and J. U. Kang, "GPU-accelerated non-uniform fast Fourier transform-based compressive sensing spectral domain optical coherence tomography," Opt. Express **22**(12), 14871–14884 (2014).
14. W. Jung, B. Kao, K. M. Kelly, L. H. L. Liaw, J. S. Nelson, and Z. Chen, "Optical coherence tomography for *in vitro* monitoring of wound healing after laser irradiation," IEEE J. Sel. Top. Quantum Electron. **9**(2), 222–226 (2003).
15. A. T. Yeh, B. Kao, W. G. Jung, Z. Chen, J. S. Nelson, and B. J. Tromberg, "Imaging wound healing using optical coherence tomography and multiphoton microscopy in an *in vitro* skin-equivalent tissue model," J. Biomed. Opt. **9**(2), 248–253 (2004).
16. M. T. Tsai, C. H. Yang, S. C. Shen, Y. J. Lee, F. Y. Chang, and C. S. Feng, "Monitoring of wound healing process of human skin after fractional laser treatments with optical coherence tomography," Biomed. Opt. Express **4**(11), 2362–2375 (2013).
17. E. C. E. Sattler, K. Poloczek, R. Kästle, and J. Welzel, "Confocal laser scanning microscopy and optical coherence tomography for the evaluation of the kinetics and quantification of wound healing after fractional laser therapy," J. Am. Acad. Dermatol. **69**(4), e165–e173 (2013).
18. C. A. Banzhaf, B. S. Wind, M. Mogensen, A. A. Meesters, U. Paasch, A. Wolkerstorfer, and M. Haedersdal, "Spatiotemporal closure of fractional laser-ablated channels imaged by optical coherence tomography and reflectance confocal microscopy," Lasers Surg. Med. **12**, 22386 (2015).
19. P. Gangatirkar, S. Paquet-Fifield, A. Li, R. Rossi, and P. Kaur, "Establishment of 3D organotypic cultures using human neonatal epidermal cells," Nat. Protoc. **2**(1), 178–186 (2007).
20. T. Matsui and M. Amagai, "Dissecting the formation, structure and barrier function of the stratum corneum," Int. Immunol. **27**(6), 269–280 (2015).
21. M. Varkey, J. Ding, and E. E. Tredget, "Superficial dermal fibroblasts enhance basement membrane and epidermal barrier formation in tissue-engineered skin: implications for treatment of skin basement membrane disorders," Tissue Eng. Part A **20**(3-4), 540–552 (2014).
22. E. Catalano, A. Cochis, E. Varoni, L. Rimondini, and B. Azzimonti, "Tissue-engineered skin substitutes: an overview," J. Artif. Organs **16**(4), 397–403 (2013).
23. S. V. Murphy and A. Atala, "3D bioprinting of tissues and organs," Nat. Biotechnol. **32**(8), 773–785 (2014).
24. A. Atala and J. J. Yoo, *Essentials of 3D Biofabrication and Translation* (Academic Press, 2015), Chap. 22.
25. S. H. Ahn, H. J. Lee, J. S. Lee, H. Yoon, W. Chun, and G. H. Kim, "A novel cell-printing method and its application to hepatogenic differentiation of human adipose stem cell-embedded mesh structures," Sci. Rep. **5**, 13427 (2015).
26. K. M. Kennedy, L. Chin, R. A. McLaughlin, B. Latham, C. M. Saunders, D. D. Sampson, and B. F. Kennedy, "Quantitative micro-elastography: imaging of tissue elasticity using compression optical coherence elastography," Sci. Rep. **5**, 15538 (2015).

1. Introduction

As laser technology is advanced, laser therapy has become a common way of treating various dermatological conditions such as wrinkles, melasma, and lentigo that are induced by aging [1, 2]. The recent interest in appearance management has led to the rapid growth of the global laser market in the medical and aesthetic fields, which is expected to reach nearly $815 million in 2015 [3]. Although laser therapy is widely utilized in skin treatment, there is still a need for further improvement and development in order to provide optimal care that reflects different skin structure and biological composition, such as thickness, collagen content, and

density. In particular, dynamic and quantitative observation of laser-tissue interaction is important to accomplish customized skin therapy while preventing side-effects such as hyperpigmentation, redness, and burning [4, 5].

In order to study wound healing processes in laser irradiated tissue, various monitoring methods have been tried. Histology is still the golden standard for investigating tissue structure in the biological and medical field, but it has inherent limitations when applied to dynamic studies due to its destructive treatment of specimens. Optical imaging techniques, including reflectance confocal microscopy, fluorescence microscopy, and second harmonic microscopy, have also been considered as promising tools for investigating structural change of tissue. Each optical imaging modality has clearly visualized biological components such as keratinocyte, melanocyte, and collagen, and was applied to investigate the collagen-elastic fiber interaction during a photo-aging process [6–9]. Even though most microscopic techniques provide high-contrast, and cellular resolution imaging, there still remains some critical restriction in monitoring laser irradiated tissue regions due to its shallow penetration depth and narrow field of view. Considering that the depth of laser treated regions is more than 1 mm, most optical imaging technologies are beyond deep tissue imaging.

For this reason, optical coherence tomography (OCT) has emerged as the most appropriate candidate for studying skin regeneration. In fact, OCT equips optimal imaging characteristics for dynamic skin monitoring, because it offers cross-sectional, high-resolution, real-time tissue imaging in a non-invasive manner [10, 11]. Unlike most optical imaging techniques, OCT does not require any contrast agent or labeling process. The imaging penetration depth of typical OCT is around 2-3 mm which fortunately corresponds to the depth range of common laser treatment. Recently there have been dramatic advances of OCT technology in terms of imaging speeds. Thus, current high-speed OCT systems present 3-D volumetric imaging in real time which is suitable for applying to *in vivo* study with less motion artifact. In addition, fast signal processing algorithms and high-speed computational platforms, including digital signal processors or graphical processing unit (GPU), accelerate to realize 4D OCT [12, 13]. To date, OCT has been intensively utilized in biomedical applications for diagnosing a variety of tissue abnormalities, but only a few OCT studies have been specifically targeted for laser wound healing monitoring, despite a clear need and enough potential. Even previous OCT studies describing the regeneration process of skin showed only preliminary results excluding quantitative analysis or light-tissue interaction based on laser irradiation parameters [14–18].

Here, we demonstrate the feasibility of three-dimensional OCT for quantitative tissue monitoring after laser irradiation. In this study, we hired engineered skin which reflected that animal study is currently prohibited in the cosmetic field due to ethical issues. Engineered skin is also a good research platform to evaluate wound healing processes due to its good manipulability and an experimental reliability that is higher than animal models. The customized engineered skin was fabricated to mimic the diversity of human skin and was then irradiated at various laser parameters. Quantitative recovery over time was investigated by OCT imaging and intensive image processing.

2. Materials and methods

2.1 Optical coherence tomography (OCT) system

We developed a spectral domain optical coherence tomography (SD-OCT) to monitor wound healing processes as shown in Fig. 1. A super-luminescent diode (SLD, EXALOS Inc.) with a 50 nm full-width half-maximum spectral bandwidth at the center wavelength of 840 nm, was incorporated into the SD-OCT system, which provided ~6 μm axial resolution in the tissue. The emitted light from SLD was coupled into the 2×2 fiber coupler and divided into two optical paths, reference and sample arm. The sample arm consisted of a collimator, beam expander, dual-axis galvanometer scanners and an objective lens to image tissue specimens

with ~15 μm lateral resolution. The reflected lights from the sample and reference arms were interfered with the 2 × 2 fiber coupler and detected by a customized spectrometer consisting of a transmission type diffraction grating (1145 lines/mm, Wasatch Photonics), a focusing lens, and a 1024-pixel line scan camera (SUI Goodrich). The captured interference signal from the line scan camera was digitized by a frame grabber (National Instruments), processed by FFT, and converted to a log intensity profile for plotting the depth information. OCT images accumulated by 1000 axial scans were visualized at a rate of ~20 frames/s. The 3D OCT image was constructed by a 500 OCT image set. The corresponding speed for a single three-dimensional volumetric image was ~25 second.
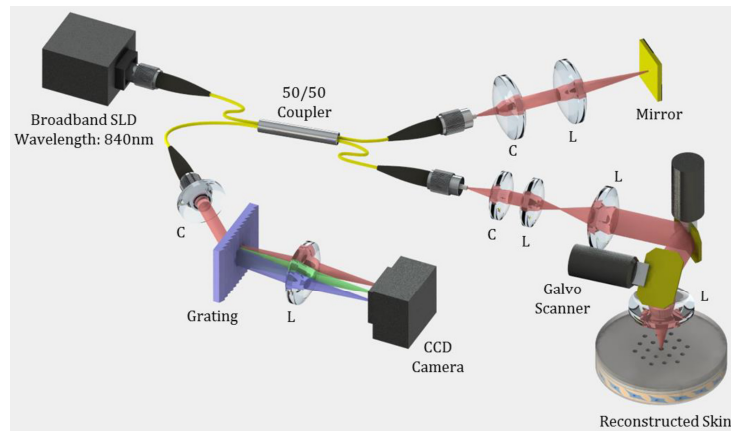

Fig. 1. Schematic diagram of the SD-OCT system used for observing skin regeneration. SLD: super-luminescent diode, C: Collimator, L: Lens.

2.2 The preparation of engineered skin

In our study, customized engineered skins consisting of dermal and epidermal layers were developed as presented in Fig. 2. The major fabrication steps of engineered skin include (1) the construction of the acellular layer with collagen compound, as well as the cellular layer containing fibroblast for a dermal layer, (2) seeding of keratinocytes on the second dermal layer, and (3) proliferation and differentiation for an epidermal layer [19]. Through the above procedure, two dermal layers were cultured in a medium for seven days at 37 °C, 5% CO_2, and the epidermal layer was seeded by human epidermal neonatal keratinocytes on the second dermal layer. In order to proliferate the keratinocytes, the layered skin was then submerged in a culture medium for another seven days. Lastly, the engineered skin was completed after the procedure of air exposure for epidermal differentiation.
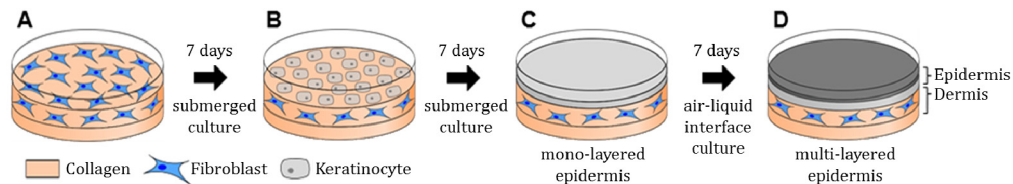

Fig. 2. Schematic of engineered skin preparation procedure. (A) Dermal layer of engineered skin was composed of acellular dermis containing collagen, and cellular dermis containing collagen and fibroblast. (B, C) After seven days, keratinocytes were cultured on the surface of a dermal layer. The epidermal monolayer formed as keratinocytes were proliferated and differentiated. After monolayer development, the submerged medium removed except the bottom of engineered skin for air exposure. (D) The epidermal multi-layer constructed using air-liquid interface culture.

Figure 3(A) shows the H&E stained engineered skin structure that is a proliferation of the epidermis with keratinocyte and of dermis with fibroblast. The histology indicates that the engineered skin has two main layers (epidermis and dermis), distinguishable by the extent of staining. The multi-layers of the epidermis are composed of stratum corneum and epidermal keratinocyte. The dermis is located below the epidermis multi-layers, and is composed of dermal fibroblast and organized extracellular matrix. Figure 3(B)-3(D) shows confocal microscope images of the engineered skin. Figure 3(B) represents the proliferation of keratinocyte, which is a primary composition of epidermis basement using proliferation marker, Ki-67. The green color of Ki-67 demonstrates that the engineered skin has a well-grown epidermis, and it shows a usual pattern of epidermis stem cell proliferation. In Fig. 3(C), the junctional protein, Laminin-5 strongly attaches to a junction protein that is mainly expressed in the epidermis-dermis junction. The clear red color indicates that the engineered skin grows in a similar way to human skin. Figure 3(D) represents the differentiation of keratinocyte in engineered skin using differentiation markers; involucrin and filaggrin. Those markers are an indicator of how similar the engineered skin is to human skin. The blue marker, made by DAPI (4', 6-diamidino-2-phenylindole) staining shows the nucleus of keratinocyte. It demonstrates that the nucleus of keratinocyte gradually disappears to the top of the epidermis as differentiation of keratinocyte is processed.
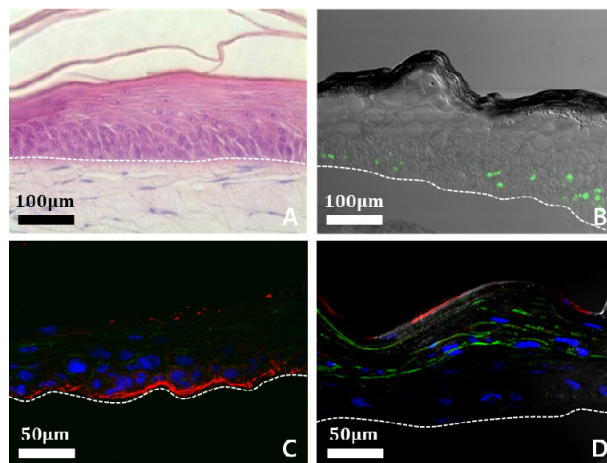

Fig. 3. Analysis of constitutive of engineered skin structures using a confocal microscope; epidermis is above the white dotted line and dermis is below the line. (A) Cross-sectional H&E stained image of engineered skin. (B) Proliferation of keratinocyte is shown by using proliferation marker, Ki-67 (green). (C) Epidermis-dermis junction is shown by using junctional protein, Laminin-5 (red). (D) Differentiation of keratinocyte is shown by using differentiation markers, involucrin (green) and filaggrin (red). Nucleus of keratinocyte demonstrates using DAPI staining method (blue).

2.3 Laser irradiation and OCT imaging

The injury model was produced by laser ablation on the engineered skin. The fractional CO_2 laser resurfacing (Lutronic Co., Ltd) was used by adjusting several irradiation conditions, such as pulse energy, spot density, and the irradiation area. The pulse energy of the laser for the major experiment was treated at 40, 80, and 120 mJ/cm^2. The laser irradiated an 8 mm circular region, and the corresponding spot density was 100 spots/cm^2.

We prepare two groups of engineered skin samples which were irradiated by resurfacing laser to compare both OCT data and fixed reference data. After laser irradiation, the first group was cultured continuously in a medium to observe the skin regeneration process every 6 hours using the 3D OCT system. The second group was fixed by using formalin solution every 6 hours. For histological analysis, engineered skin samples were embedded in optimal

cutting temperature compound for cryostat sectioning, or in paraffin for hematoxylin and eosin staining. Each sample slice was captured using a digital camera integrated optical microscope (Olympus).

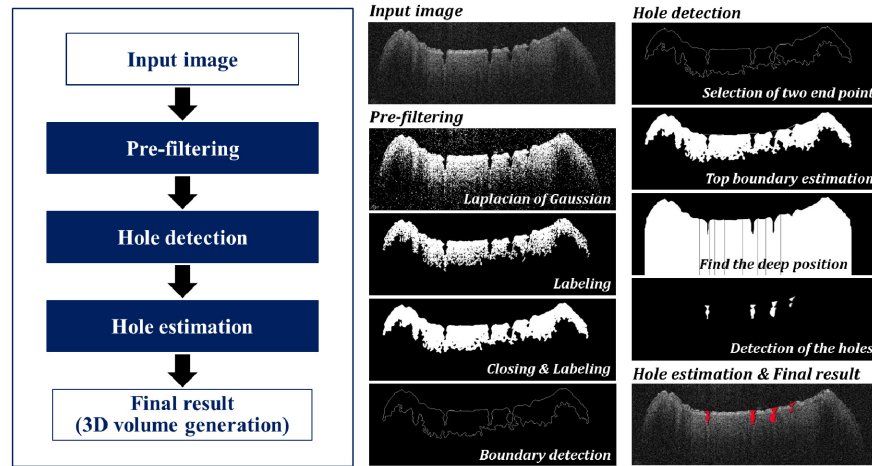*2.4 Image processing and quantification*

Fig. 4. The automatic segmentation algorithm for quantitative analysis of skin regeneration. The whole process is consisted of 'Pre-filtering', 'Hole detection', and 'Hole estimation'.

To quantify the skin regeneration process, we developed an automatic segmentation algorithm using MATLAB, as shown in Fig. 4. The automatic segmentation involves three steps: (1) pre-filtering, (2) hole detection, and (3) hole estimation. Firstly, we applied the Laplacian of Gaussian filter on an original gray-scale OCT image to remove noise. Using the Otsu's threshold method, the filtered gray-scale image is converted into binary values. The connected-component labeling and the morphological close operation are used to find the gross morphology of the irradiated skin. These two operations are repeated until the skin morphology no longer changes. Next, we apply the Sobel operator to detect the boundary while preserving the boundary of the skin damaged due to laser irradiation. Using the curve fitting method, we estimate the original skin boundary before laser irradiation in which the skin does not have holes. Combining these two boundaries provides us the enclosed objects which can be holes or local fluctuations such as wrinkles. Regarding the depth of each detected object, we determine whether the detected object is a hole or not. Lastly, after detection, the volume of a hole is measured by repeating the routines as mentioned above for an entire image set and adding the areas together.
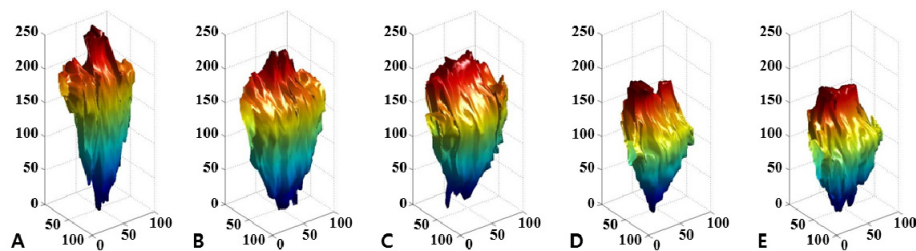

Fig. 5. Volumetric image of irradiated hole. The images were reconstructed by automatic segmentation. The engineered skin was irradiated by 80 mJ/cm^2 laser power, and monitored every 6 hours; (A) 0 hours, (B) 6 hours, (C) 12 hours, (D) 18 hours, and (E) 24 hours after laser treatment was conducted.

All of the cross-sectional images corresponding to the hole were segmented, and they were accumulated to reconstruct a three-dimensional hole according to corrected value between the voxel and actual distance. Figure 5 shows the result of the image reconstruction, and visualizes intuitive and quantitative data of the wound regeneration process. Consequently, the values for the wound volume are automatically calculated to observe the morphological change, and the results are quantified and visualized for each observation time of 6 hours.

3. Results

3.1 Correlation study of skin regeneration over time

The recovery process of laser treated skin was monitored by OCT and compared to corresponding histology and microscopic images over time. Figure 6 shows the representative correlation data set over 18 hours after laser irradiation. Conventional observation using a microscope and histology provides the surface view and cross-sectional view, respectively. OCT images offer both surface and cross-sectional morphology together, and show strong similarities to images acquired from existing methods. All OCT images were acquired from the same engineered skin; thus it was possible to identify the dynamic variation of very thin remaining tissue structure, after laser irradiation, without damage, as presented in Fig. 6. The image acquisition time of the OCT system was fast enough to monitor and maintain the engineered skin while minimizing denaturation.
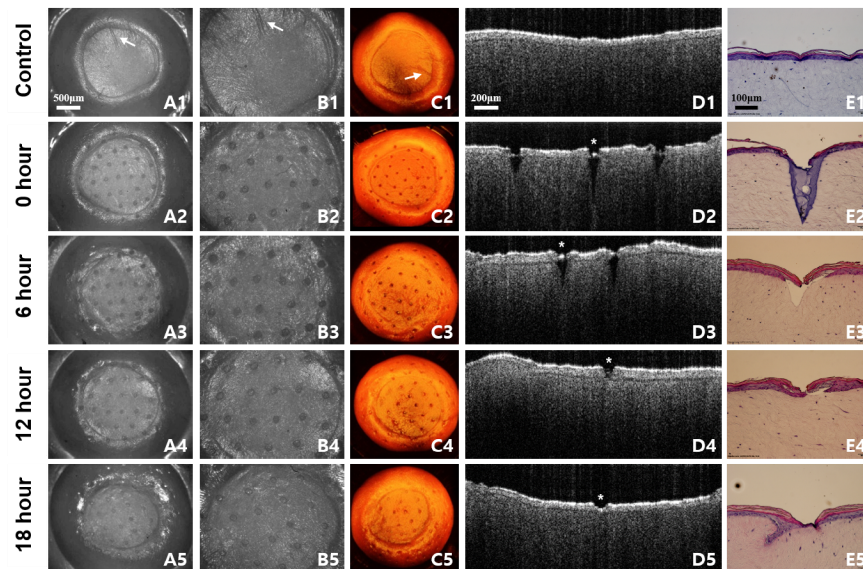

Fig. 6. The recovery process of engineered skin over 18 hours after laser irradiation. The samples are irradiated by 40 mJ/cm^2 laser power monitored every 6 hours. No laser irradiated samples (A1-E1) show the difference compared to laser irradiated samples (A2-E2). (A, B) Microscopic images are corresponding to 3D OCT images in (C). The white arrow indicates the correlation of 3D OCT images compared to microscope images. (D) Cross-sectional 2D OCT images demonstrate similar aspects of H&E stained images in (E). The white star indicates the corresponding location of OCT image to H&E stained image.

In the *en-face* OCT image, shown in column C of Fig. 6, the laser irradiated regions on the engineered skin are denoted as round spots with regular spacing. The structure of *en-face* OCT images including spots and even the scratch (indicated by an arrow) was strongly coincident with light microscopic images as presented in column A and B of Fig. 6. The boundary of irradiated spots in *en-face* OCT images has gradually recovered over time, and adjacent irradiated spots even in the same engineered skin have a different healing process.

This indicates that the tissue recovery depends on the location of engineered skin, and is also very sensitive to tissue structure as well as irradiation conditions such as exposure angle and distance. In B-mode OCT image, the skin layers and laser irradiated zone were clearly identified. As shown in Fig. 6(D2), 6(E2), the collagen of the engineered skin was denatured, and a V-shaped wound was formed immediately after the laser irradiation. After 6 hours, the stratum corneum and epidermis were recovered as shown in Fig. 6(D3), 6(E3). Our results show that the irradiated zone in the dermis recovered more slowly than that in the epidermis at a given irradiation condition and tissue structure. The irradiated zone was completely filled and recovered within 24 hours. The research protocol including comparison study, shown in Fig. 6, was repeated for the entire experiment.

3.2 Wound healing in accordance with epidermal thickness

We evaluated the laser-induced wound healing in the different engineered skins. In this study, the two types of engineered skin with different epidermis thicknesses were prepared and treated at the same laser dosage, 120 mJ/cm^2. The laser irradiated region was then imaged with 3D OCT, segmented, and its morphological change at different time points were compared. The segmented OCT image acquired from the central location of the laser treated zone of each skin are visualized in Fig. 7(A). The OCT image of the wound shows that light energy penetrated more deeply at the thin epidermal skin. OCT images also show that the width of an irradiated zone at the epidermal layer is narrower than that at the dermal layer. Irradiated light initially interacted with the epidermis of skins which has a role as a resistance against light energy. Through this experiment, we confirm that the epidermal layer has higher resistance compared to the dermal layer when the light propagates into the engineered skin. The reason appeared different value of resistance is that stratum corneum, the outmost layer of the epidermis, has a fully differentiated and tightly bound keratinocyte structure embedded in the intercellular lipids [20]. This unique structure called, 'bricks and mortar' forms a physiological barrier of the skin and regulates the entrance of the external substances. Due to physical characteristics of stratum corneum, the thickness of epidermis affects the degree of skin penetration by the light. Quantitative results presented in Fig. 7(B) show that the tissue regeneration of thin epidermal skin is more active compared to one of thick epidermal skin. This means that the tendency of wound recovery at given laser irradiation condition is proportional to the entire area of tissue exposed by laser irradiation.
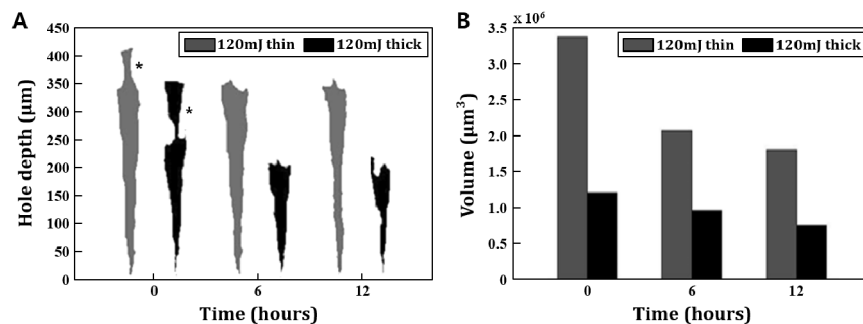

Fig. 7. Comparison of the relationship between epidermis thickness and wound depth with volume. The grey one indicates thin epidermal engineered skin, and the dark one is thick epidermal skin. (A) The thin epidermal engineered skin has an epidermal layer of 50 μm (from 350 μm to 400 μm), and the initial penetrated hole depth after layer irradiation is about 400 μm. In thick epidermal engineered skin, the epidermal thickness is about 100 μm (from 250 μm to 350 μm) and the initial penetrated hole depth is about 350 μm. The black star indicates the irradiated epidermal area. (B) The initial hole volume after irradiation is 3.3 million μm^3 in thin epidermis skin and 1.2 million μm^3 in the thick sample.

3.3 Wound healing in accordance with exposure energy

We investigated the wound healing process in varying the laser exposure power. In order to maintain experimental analogy, engineered skins were pre-scanned by OCT and their structures were analyzed. Engineered skins with around 70 μm epidermal thickness were selected, and irradiated by three different laser energy levels, 40, 80 and 120 mJ/cm^2. Finally, sorted skins were then imaged by OCT again to monitor tissue recovery every 6 hours for a day. For the quantitative analysis of the wound zone, the same image processing protocol described in the previous chapter was applied and repeated.
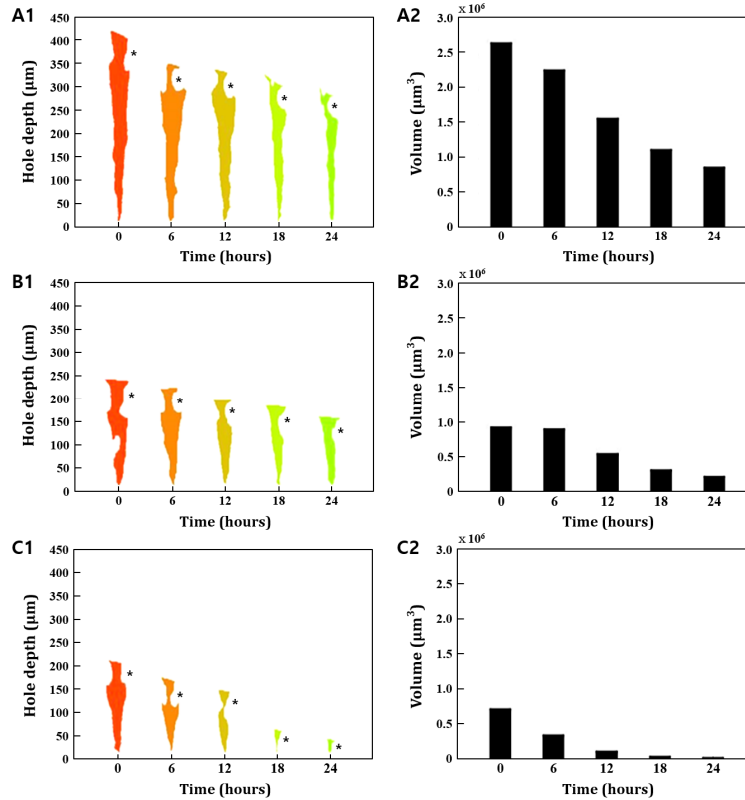

Fig. 8. Comparison of the relationship between different laser powers and wound depth with volume. (A1) The hole depth after irradiation is about 420 μm in 120 mJ/cm^2 laser power, (B1) 240 μm in 80 mJ/cm^2 laser power, and (C1) 220 μm in 40 mJ/cm^2 laser power. (A2) The volume after irradiation is about 2.6 million μm^3 in 120 mJ/cm^2 laser power, (B2) 0.9 million μm^3 in 80 mJ/cm^2 laser power, and (C2) 0.7 million μm^3 in 40 mJ/cm^2 laser power. The black star indicates the irradiated epidermal area.

As presented in Fig. 8, the laser irradiated zone of engineered skins was proportional to the light energy applied. Our results showed that the recovery time of engineered skin varied by the amount of light energy. In 120 mJ/cm^2 dosage, the recovery of epidermis was faster than in the dermis layer. On the other hand, the tendency of recovery at the dermis and epidermis was opposite when the relatively low energy, 40 mJ/cm^2, was applied. In 80 mJ/cm^2 dosage, the recovery process was very slow for the first 6 hours and then tends to be healed steadily every hour. As shown in Fig. 8(B1), the recovery time in 80 mJ/cm^2 has a uniform healing process at each epidermal and dermal layer. Through experimental results, we found that light energy influences the variation of regional recovery between the dermis and epidermis. This effect indicates that the adjustment of laser exposure energy is essential to adjust balanced tissue recovery at skin layers as well as the tissue recovery time. Considering

the morphological change of a segmented OCT image, we also found that the recovery process of the laser irradiated zone is more active in the horizontal direction than in the vertical direction. As mentioned, the advantage of OCT in wound healing studies is the dynamic imaging capability. Thus, the graphical visualization of the healing process using volumetric OCT images offers comprehensive knowledge for better understanding tissue recovery and unique information, such as regional observation, which cannot be acquired by existing monitoring tools.

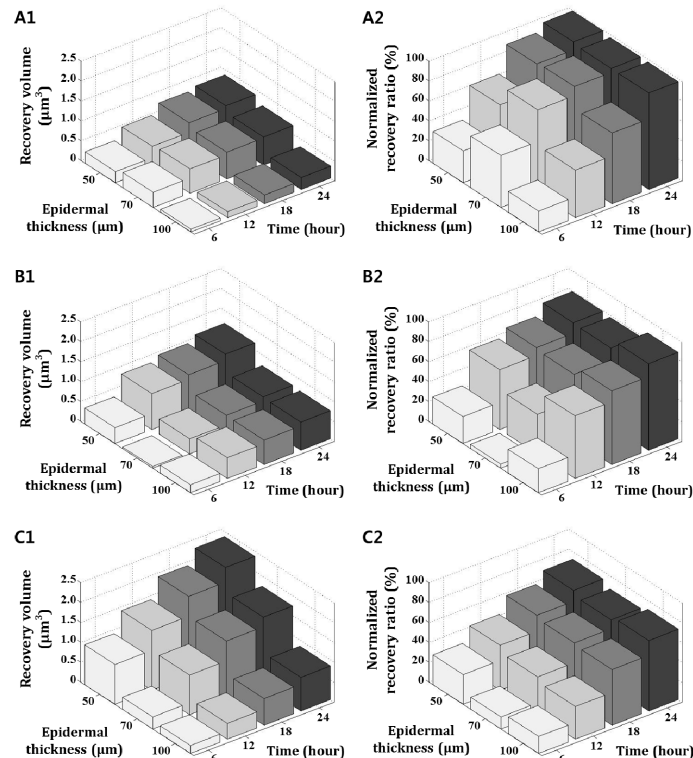*3.4 Wound healing in accordance with epidermal thickness and exposure energy*

Fig. 9. Comparison of the change of recovery volume and normalized recovery ratio according to a variation of laser exposure power and epidermal thickness. The recovery volume indicates the difference between initial and the volumes which were measured every 6 hours. Similarly, the normalized recovery ratio was measured every 6 hours and indicates the extent of the wound that was recovered from the initial wound. (A1) The recovery volume and (A2) the recovery ratio of after 40 mJ/cm^2 laser exposure, (B1) and (B2) after 80 mJ/cm^2 laser exposure, (C1) and (C2) after 120 mJ/cm^2 laser exposure.

In the previous experiment, we found that the tissue recovery was varied by the light exposure energy. We also found that the wound healing process differed by skin thickness as well. Most current protocols of laser treatment in the clinic, laser exposure parameters are adjusted with less consideration about the skin thickness and structure. It is because of a lack of tissue monitoring tools. In order to approach a more accurate and realistic experiment, we considered experiment variations in both laser exposure energy and tissue structure. In this study, three kinds of engineered skins were fabricated which have a different epidermal thickness, 50, 70, and 100 μm. Each skin was equally irradiated at 40, 80, and 120 mJ/cm^2, and its recovery process was then monitored by OCT.

Figure 9 presents the recovered volume (first column) and normalized recovery ratio (second column) to verify the relation between two experimental variations. To derive the recovery volume, the irradiated zone in the engineered skin was imaged by OCT, segmented

and calculated its increment every 6 hours during 24 hours. The increment by time was plotted in the first column of Fig. 9. The recovery ratio was derived from the comparison between the initial volume and recovered volume of the laser irradiated zone as each time point. Our results clearly explain that different skin structure is closely related to tissue recovery. The recovered volume of the irradiated zone at 50 μm epidermis skin was larger than other skins with thicker epidermal layers. As we described in Fig. 7, this is because the thickness of the epidermis is very sensitive to light-tissue interaction and has effects on the penetration of light energy. Therefore, thin epidermis skin had a larger irradiated area with a deeper dermis region and the recovered volume was relatively larger. This tendency is more obvious when exposed light energy is increased. On the other hand, the overall recovery ratio has less deviation by skin structure. In particular, the recovery ratio is very similar regardless of epidermal thickness when time goes by. Through this experiment, we found that both the structure of the skin and the variable of laser exposure have a strong influence on the volume of irradiated as well as recovered zone. However, the influence of the recovery ratio is more sensitive to the laser exposure power.

4. Discussion

OCT is a proper imaging modality to monitor the wound healing process, because it provides morphological change of tissue, non-invasively and dynamically. As OCT technology is advanced, it is also possible to observe volumetric and quantitative healing process of wound region. Even though OCT has strong potential to be utilized to wound healing study, only few researches have been reported for laser wound monitoring as shown in Table 1 [14–18].

Table 1. Comparison of laser wound healing study based on OCT.

	Laser Type (Wavelength)	Laser Dosage	Irradiated Area (Diameter)	Subject	Recovery Time	Monitoring Tool
Our Study	CO_2 Laser (10,600 nm)	40, 80, and 120 mJ/cm^2	~100 μm	Engineered Skin	1~2 days	OCT
W. Jung, et al. [14]	Nd:YAP Laser (1,341 nm)	25 and 35 J/cm^2	~1.5 mm	Engineered Skin	~7 days	OCT
A. T. Yeh, et al. [15]	Nd:YAP Laser (1,341 nm)	20 J/cm^2	~1.5 mm	Engineered Skin	~7 days	OCT MPM[a]
M. T. Tsai, et al. [16]	Erbium-doped Fiber Laser (1,550 nm)	15, 20, and 25 mJ/cm^2	~200 μm	Human Skin	6 days	OCT
	CO_2 Laser (10,600 nm)		~150 μm		14 days	
E. C. E. Sattler, et al. [17]	CO_2 Laser (10,600 nm)	8 and 16 W	~ 400 μm	Human Skin	7~14 days	OCT CLSM[b]
C. A. Banzhaf, et al. [18]	CO_2 Laser (10,600 nm)	5, 15, and 25 mJ/cm^2	~100 μm	Human Skin	2~7 days	OCT RCM[c]

[a]Multi-photon Microscopy
[b]Confocal Laser Scanning Microscopy
[c]Reflectance Confocal Microscopy

One of interest in tissue regeneration study is to investigate the recovery time of wound region. As previous works present, the tissue recovery is varied by the targeted tissues as well as the laser irradiation parameters such as laser dosage, duration, and exposed area. Our previous and current works utilized the engineered skin, but it showed different recovery time [14, 15]. As aforementioned, the laser treated region in this study was mostly recovered

within 1~2 days which was faster than one in our previous studies, 7 days. It is because that laser energy exposed in previous work, 20~35 J/cm^2 was much higher than what we used in this study, 40, 80, and 120 mJ/cm^2. Entire area of laser irradiated region is also crucial component to make the different recovery time. Thus, the shorter recovery time presented in this study is reasonable. On the other hand, M. T. Tsai, *et al*. and C. A. Banzhaf, *et al*. used human skin rather than engineered skin. Even though they hired similar laser irradiation condition to our study, the wound healing time shows the big disparity [16, 18]. It indicates the engineered skin is structurally analogous to human skin, but it has still restriction to fully mimic the human skin. In general, most engineered skins have simple skin structure which is composed of essential elements such as fibroblast, keratinocyte, and collagen. Whereas human skin contains additional extracellular matrix and other cells which forms tight junctions between biological components [21]. In human skin, wound healing process involves systemic and complex events including hemostasis, cell migration, matrix deposition and tissue remodeling [22]. However, the tissue regeneration in engineered skin having basic structure and loose biological junction is mainly governed by simplified process, cell proliferation and remodeling. Therefore, faster laser wound recovery in this study can be explain by structural and functional difference as well as different healing events between engineered skin and human skin. Nowadays, tissue engineering technology is getting advanced combined with other relevant technologies including stem cell, bio-material and bio-printing [23–25]. When the engineered skin is mature and closer to human skin, it is believed that wound healing study combined with engineered skin and OCT quantification could be emerging research platform with high reliability.

5. Conclusion

To date, the golden standard to observe a structural change of wound recovery has been to use histological sectioning and a light microscope. Even though the histological analysis is routine laboratory procedure, it has inherent limitations when the experiment involves quantitative inspection as well as dynamic monitoring. In contrast, volumetric OCT imaging clearly visualizes morphological variation of wounds and healed regions in a non-invasive fashion. Through our experiment, we found that OCT delivers comprehensive information for the better understanding of tissue regeneration, such as the regional recovery by skin layer and the recovery ratio with different laser irradiation parameters.

As OCT technology matures, numerous OCT methods can be applied to further tissue engineering study. Optical coherence elastography (OCE), an expansion of OCT, enables to the measurement of tissue stiffness and mapping onto typical OCT images [26]. When OCE is applied to image laser-induced wound recovery, it is a very useful tool for investigating the fibrosis surrounding the hole during a light-tissue interaction. The enhancement of imaging speed and penetration depth can also build up the potential of OCT toward *in vivo* human studies. The functional handheld imaging probes would be the last step in realizing the OCT-guided laser treatment.

In conclusion, we have demonstrated quantitative OCT in a laser wound recovery study. Experimental results showed that the wound healing process is active in the vertical direction, and recovery time varies by the tissue structure as well as the irradiation condition. We also confirm that OCT is the most promising tool for monitoring the wound healing process, when it is integrated with other contrast, such as stiffness and polarization.

Acknowledgments